PERGAMON

International Journal of Solids and Structures 37 (2000) 3231–3251

INTERNATIONAL JOURNAL OF SOLIDS and STRUCTURES

www.elsevier.com/locate/ijsolstr

On the electroelastic behaviour of a thin piezoelectric actuator attached to an infinite host structure

X.D. Wang [1], S.A. Meguid*

Engineering Mechanics and Design Laboratory, Department of Mechanical and Industrial Engineering, University of Toronto, 5 King's College Road, Toronto, Ont., M5S 3G8 Canada

Received 7 July 1998; in revised form 9 April 1999

Abstract

In this paper, we examine the coupled electromechanical behaviour of a thin piezoceramic actuator embedded in or bonded to an elastic medium under inplane mechanical and electrical loadings. The actuator is characterized by an electroelastic line model with the poling direction being perpendicular to its length. The theoretical formulations, governing this electromechanically coupled problem, are based upon the use of singular integral equations in terms of an interfacial shear stress. A square-root singularity of the resulting shear stress is found at the tips of the actuator. A new shear stress singularity factor (SSSF) was then obtained by solving these singular integral equations using Chebyshev polynomial expansions. Typical examples are provided to show the effect of the geometry of the actuator, the material combination and interfacial debonding upon the shear stress singularity factor.

1. Introduction

With the emergence of new piezoceramic materials, the concept of using a network of piezoelectric actuators and sensors to form a self controlling and self monitoring smart system in advanced structural design has drawn considerable interest among the research community (Gandhi and Thompson, 1992; Dosch et al., 1995; Varadan et al., 1993). Piezoelectric sensors, which are attached to a structure, can convert the strain of the structure into electric signals to monitor the deformation of the host structure. In a reverse procedure, an applied electric field to a piezoelectric actuator will result in a mechanical deformation of the actuator, which will in turn deform the host structure through load transfer at the

* Corresponding author Tel.: +001-416-978-5741; Fax: +001-416-978-7753.
E-mail address: meguid@mie.utoronto.ca (S.A. Meguid).
[1] Current address: Department of Mechanical Engineering, University of Alberta, Edmonton, Alberta T6G 2G8, Canada.

0020-7683/00/$ - see front matter
PII: S0020-7683(99)00118-3

interface to generate axial forces or bending moments on the structure. In these smart systems, both electromechanical coupling and material inhomogeneity are involved. The designers of such systems are constantly faced with the challenge of establishing suitable shapes and positions of actuators to provide high-performance structures.

One of the most fundamental issues in using integrated actuators in smart structures is to determine the actuation effects being transferred from the actuators to the host and the resulting overall structural response. Another important aspect related to the design of the integrated smart system is the determination of interfacial stresses that may result in failure of the structure integrity. An accurate assessment of the coupled electromechanical behaviour of an integrated structure would, therefore, require the determination of the local stress distribution in smart structures involving piezoelectric actuators/inhomogeneities.

In view of its importance to the development of advanced structures, the subject of piezoelectric actuator has received attention from the scientific community. These include the work of Deeg (1980) and Benveniste (1992) on the single elliptical (ellipsoidal) inhomogeneity in unbounded piezoelectric materials using the Green's function approach; Dunn and Taya (1993) on the determination of the effective properties of piezoelectric composites using different micromechamcial models; and the work of Jain and Sirkis (1994) and He et al. (1994) on damage analysis of piezoceramics. However, relatively few studies have been made to investigate the local stress field around piezoelectric actuators in smart structures. Crawley and de Luis (1987) first analyzed a beam-like structure with surface bonded and embedded thin sheet piezoelectric actuators to study the stresses transfered by the actuator to the host beam. In that analysis, the axial stress in the actuator was assumed to be uniform across its thickness and the host structure was treated as a Bernoulli–Euler beam. The result indicated that, for a perfectly bonded actuator, the shear stress between the actuator and the host beam was transfered over an infinitesimal distance near the ends of the actuator. Crawley and Anderson (1990) further developed a Bernoulli–Euler model of a piezoelectric actuator by considering the linear stress distribution along its thickness. These models are useful in determining the structural response of composite beams. However, they are unsuitable for the prediction of the local stress distribution near the ends of an actuator, because of the limits imposed on the field by the use of Bernoulli–Euler simplification.

Im and Atluri (1989) modified the actuator model presented by Crawley and de Luis (1987) to investigate a beam with a piezoelectric actuator under general loading. Both the axial and the transverse shear forces in the beam were considered in formulating the governing equations. A refined actuator model based on the plane stress condition was presented for a beam structure with symmetrically surface-bonded actuator patches (Lin and Rogers, 1993a, 1993b). The stress distribution in the actuators and the host beam was determined by using an approximated axial stress field with a parabolic profile in the direction of the thickness of the actuator. The result indicated that this model was in good agreement with the finite element results.

The objective of the present paper is to provide an analytical model of the coupled electromechanical behaviour of a thin-sheet piezoceramic actuator embedded in or bonded to an elastic medium under inplane mechanical and electrical loadings. This loading condition corresponds to the case where the applied mechanical and electrical loads are uniformly distributed along the width of the structure. Since the main interest of the current study is the local stress concentration and the load transfer near the actuator, the host structure is assumed to be infinite. This represents the case where the host structure is much thicker than the actuator. The analysis is based upon the use of a one-dimensional actuator model and the solution of the resulting singular integral equations is developed in terms of an interfacial shear stress. The solution indicates that there exists a square-root singular stress field near the tips of the actuator. Two aspects of the work are accordingly examined. The first is concerned with determining the effect of the geometry, the material mismatch and electroelastic property of the actuator upon the

resulting shear stress singularity factor, while the second is concerned with the possible interfacial debonding and its effect upon the stress distribution in the composite structure.

2. Analysis of a single piezoelectric actuator

Piezoelectric actuators made of thin-sheets are commonly used in structural applications (Crawley and Anderson, 1990; Hubbard and Bailey, 1985). This type of actuator is quite thin, thus enabling the application of a high electrical intensity.

Let us now consider the plane strain problem of a thin piezoceramic actuator sheet embedded in or surface bonded to a homogeneous and isotropic elastic medium, as illustrated in Fig. 1. The half length and the thickness of the actuator are denoted a and h, respectively. It is assumed that the poling direction of the actuator is along the z-axis. An electrical field E_z is applied along the poling direction of the actuator by applying a voltage (V) between the upper and the lower electrodes of the actuator, with $E_z = V/h = (V^- - V^+)/h$.

2.1. The actuator model

Since the actuator thickness is assumed to be very small in comparison with its length, the applied electric field will mainly result in an axial deformation, and the following assumptions can be made:

(i) σ_y and u_y are uniform across the thickness of the actuator,
(ii) the interfacial shear stress (τ) transferred between the actuator and the host can be replaced by a distributed body force along the actuator, and
(iii) σ_z and σ_{yz} in the actuator can be ignored.

Based upon these assumptions, the actuator can be modelled as an electroelastic line subjected to the applied electric field and distributed axial force, τ/h, as shown in Fig. 2. The equilibrium equation of the actuator can then be expressed as

$$\frac{\partial \sigma_y}{\partial y} + \frac{\tau}{h} = 0. \tag{1}$$

Since all the load transferred between the actuator and the host can be attributed to τ, the two ends of the actuator can be assumed to be traction free, i.e.

$$\sigma_y = 0, \ |y| = a. \tag{2}$$

It should be noted that the modelling of the actuator is similar to the shear lag analysis in composite

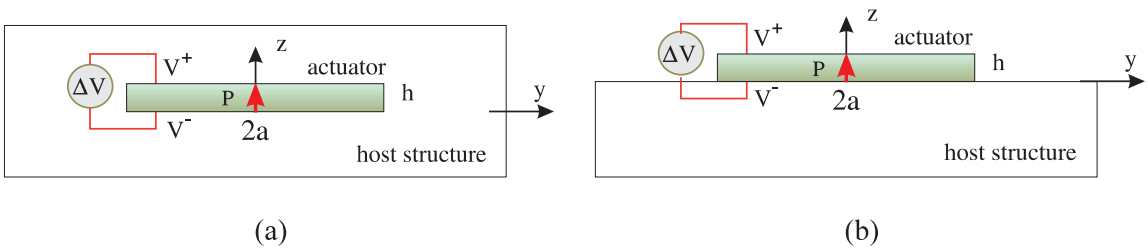

Fig. 1. Embedded and surface bonded actuators.

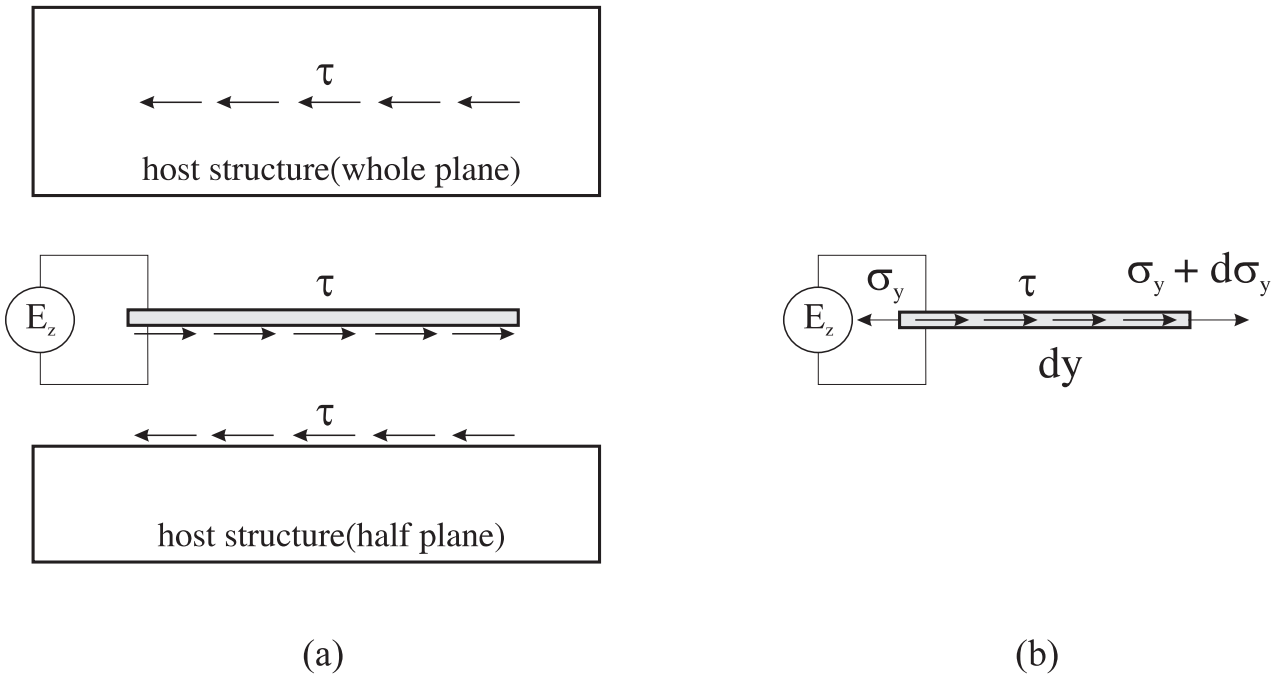

Fig. 2. Actuator model.

materials (Cox, 1952; Fukuda and Chou, 1981). However, in the current study no specific limitation is enforced upon the deformation of the matrix.

By integrating Eq. (1) and making use of Eq. (2), the axial stress in the actuator can be expressed in terms of the shear stress τ as

$$\sigma_y(y) = -\int_{-a}^{y} \frac{\tau(\xi)}{h}\,\mathrm{d}\xi, \tag{3}$$

with

$$\int_{-a}^{a} \tau(\xi)\mathrm{d}\xi = 0. \tag{4}$$

The relation between the stress, the strain and the electric fields of this actuator model can be obtained by using the following general constitutive relation:

$$\sigma_y = E_\mathrm{a}\epsilon_y - e_\mathrm{a}E_z, \tag{5}$$

where E_a and e_a are effective material constants given in Appendix A. The resulting axial strain can then be expressed in terms of τ as

$$\epsilon_y(y) = -\frac{1}{E_\mathrm{a}h}\int_{-a}^{y} \tau(\xi)\mathrm{d}\xi + \frac{e_\mathrm{a}}{E_\mathrm{a}}E_z,\ |y| < a. \tag{6}$$

2.2. Formulation of integral equations

Consider now the deformation of the host elastic medium. The applied force to the host at $z = 0$ can be expressed as:

$$f_y = \begin{cases} -\tau(y) & |y| < a \\ 0 & \text{otherwise} \end{cases}. \tag{7}$$

Based upon the fundamental solutions of a whole plane or a half plane subjected to a concentrated horizontal force (Muskhelishvili, 1953) and making use of the superposition principle, ϵ_y resulting from the applied force given by Eq. (7) can be obtained as

$$\epsilon_y(y,0)|_{\text{host}} = \frac{2}{\pi \bar{E}} \int_{-a}^{a} \frac{\tau(\xi)}{y-\xi}\, \mathrm{d}\xi, \tag{8}$$

where

$$\bar{E} = \begin{cases} \dfrac{8(1-\nu)E}{(1+\nu)(3-4\nu)} & \text{embedded} \\ \dfrac{E}{1-\nu^2} & \text{surface bonded} \end{cases}, \tag{9}$$

with E and ν being Young's modulus and Poisson's ratio of the host structure.

The compatibility of deformation between the actuator and the host structure indicates that

$$u_y|_{\text{actuator}} = u_y|_{\text{host}} \ |y| < a,\ z = 0, \tag{10}$$

which can be equivalently expressed as

$$\epsilon_y|_{\text{actuator}} = \epsilon_y|_{\text{host}} \ |y| < a,\ z = 0. \tag{11}$$

Substituting Eqs. (6) and (8) into Eq. (11) gives

$$\frac{2}{\pi \bar{E}} \int_{-a}^{a} \frac{\tau(\xi)}{y-\xi}\, \mathrm{d}\xi + \frac{1}{hE_{\mathrm{a}}} \int_{a}^{y} \tau(\xi)\mathrm{d}\xi = \frac{e_{\mathrm{a}} E_z}{E_{\mathrm{a}}},\ |y| < a. \tag{12}$$

The singular integrals, Eqs. (12) and (4), can be normalized to give

$$\left.\begin{aligned} &\int_{-1}^{1} \frac{\bar{\tau}(\zeta)\mathrm{d}\zeta}{\eta-\zeta} + q'v \int_{-1}^{\eta} \bar{\tau}(\zeta)\mathrm{d}\zeta = 1, \quad |\eta| < 1 \\ &\int_{-1}^{1} \bar{\tau}(\zeta)\mathrm{d}\zeta = 0 \end{aligned}\right\}. \tag{13}$$

The normalized shear stresses are given by

$$\bar{\tau}(\eta) = \frac{\tau(a\eta)}{\bar{p}},\ \eta = \frac{y}{a}, \tag{14}$$

with

$$q' = \begin{cases} q\dfrac{8(1-\nu)^2}{3-4\nu} & \text{embedded} \\ q & \text{surface bonded} \end{cases},$$

$$p' = \begin{cases} p\dfrac{8(1-\nu)^2}{3-4\nu} & \text{embedded} \\ p & \text{surface bonded} \end{cases} \tag{15}$$

and

$$q = \frac{\pi E}{2(1-\nu^2)E_a},\ p = qe_aE_z,\ v = \frac{a}{h}. \tag{16}$$

2.3. Solution of singular integral equations

Eq. (13) is a singular integral equation of the first kind. The solution of it involves a square-root singularity (Muskhelishvili, 1953) at $|\eta| = 1$, which corresponds to the two ends of the actuator, $|y| = a$. It can be concluded, according to the present actuator model, that the interfacial shear stress is square-root singular at the two ends of this perfectly bonded actuator.

The general solutions of $\bar{\tau}$ in Eq. (13) can be expressed in terms of the following expansions of Chebyshev polynomials,

$$\bar{\tau}(\eta) = \frac{1}{\sqrt{1-\eta^2}}\sum_{j=0}^{\infty} d_j T_j(\eta), \tag{17}$$

where T_j are Chebyshev polynomials of the first kind. By truncating the Chebyshev polynomial expansions to the Nth term and considering the boundary conditions at the following collocation points along the actuator,

$$\eta_k = \cos\frac{k-1}{N-1}\pi,\ k = 1,2,\ldots,N, \tag{18}$$

Eq. (13) reduces to

$$\sum_{j=1}^{N} d_j \frac{\sin\left(j\dfrac{k-1}{N-1}\pi\right)}{\sin\left(\dfrac{k-1}{N-1}\pi\right)}\left[1 + \frac{q'v}{\pi j}\sin\left(\frac{k-1}{N-1}\pi\right)\right] = -\frac{1}{\pi},\ k = 1,2,\ldots,N \tag{19}$$

The unknown coefficients d_j and the stress field due to the presence of the actuator can be readily determined by using Eq. (19).

To evaluate the singular behaviour of the interfacial shear stress at the tips of the actuator, we introduce a new parameter: the shear stress singularity factor (SSSF) S, defined by

$$S_r = \lim_{y\to a}[\sqrt{2\pi(a-y)}\tau(y)]$$

$$S_{\mathrm{l}} = \lim_{y \to -a} [\sqrt{2\pi(a+y)}\tau(y)]. \tag{20}$$

The SSSF at the left and the right tips of the actuator can be expressed in terms of d_j as being

$$S_{\mathrm{l}} = p'\sqrt{a\pi}\sum_{j=0}^{N}(-1)^{j}d_j$$

and

$$S_{\mathrm{r}} = p'\sqrt{a\pi}\sum_{j=0}^{N}d_j. \tag{21}$$

3. Effect of interfacial debonding

High localized stress concentration and poor interfacial conditions can result in partial debonding of the actuator from the host structure. The debonding will result in increasing the stress concentration and will therefore change the load transfer between the actuator and that host structure. In this section, attention will be focused on determining the effect of debonding upon a surface bonded actuator.

3.1. Edge debonding

The high level of shear stress at the edges of the actuator may result in an unwanted edge debonding. For a perfectly bonded actuator, when the shear stress singularity factor S reaches the 'interfacial toughness' S_{c}, edge debonding will initiate and grow. The debonded part of the actuator has zero boundary stresses. According to the present actuator model, the debonded part at the edge of the actuator will have a zero stress distribution. As a result, the effective length of the actuator is reduced from its original length to that of the bonded part. Therefore, the behaviour of an edge debonded actuator can be simulated by a shorter actuator.

3.2. Interior debonding

Debonding may also occur in the interior of the actuator. Let us consider an actuator occupying the region $t_{\mathrm{l}} < y < t_{\mathrm{r}}$, and is assumed partially debonded in $d_{\mathrm{l}} < y < d_{\mathrm{r}}$, as illustrated in Fig. 3.

By making use of the equilibrium equation Eq. (1) and the traction free condition at the two ends of the actuator, the axial stress in the actuator can be expressed in terms of the shear stress τ as follows:

$$\sigma_y(y) = \begin{cases} -\displaystyle\int_{t_{\mathrm{l}}}^{y} \frac{\tau(\xi)}{h}\,\mathrm{d}\xi & t_{\mathrm{l}} < y < d_{\mathrm{l}} \\ \sigma_{\mathrm{d}} & d_{\mathrm{l}} < y < d_{\mathrm{r}}\,, \\ \sigma_{\mathrm{d}} - \displaystyle\int_{d_{\mathrm{r}}}^{y} \frac{\tau(\xi)}{h}\mathrm{d}\xi & d_{\mathrm{r}} < y < t_{\mathrm{r}} \end{cases} \tag{22}$$

where

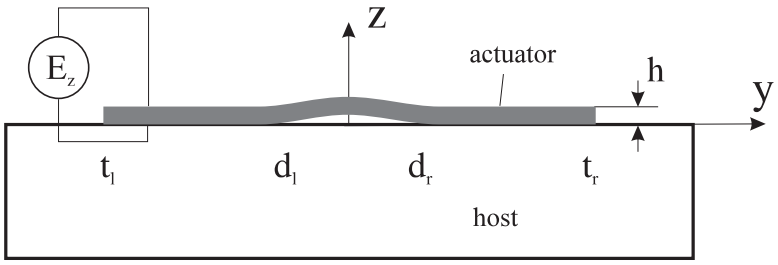

Fig. 3. Partially debonded actuator.

$$\sigma_{\mathrm{d}} = -\int_{t_{\mathrm{l}}}^{d_{\mathrm{l}}} \frac{\tau(\xi)}{h}\,\mathrm{d}\xi \tag{23}$$

is the axial stress in the debonded part of the actuator.

The resulting axial strain can then be expressed in terms of τ as

$$\epsilon_y(y) = \begin{cases} -\dfrac{1}{E_{\mathrm{a}}h}\displaystyle\int_{t_{\mathrm{l}}}^{y} \tau(\xi)\mathrm{d}\xi + \dfrac{e_{\mathrm{a}}}{E_{\mathrm{a}}}E_z & t_{\mathrm{l}} < y < d_{\mathrm{l}} \\ \dfrac{\sigma_{\mathrm{d}} + e_{\mathrm{a}}E_z}{E_{\mathrm{a}}} & d_{\mathrm{l}} < y < d_{\mathrm{r}} \\ \dfrac{1}{E_{\mathrm{a}}h}\left[\sigma_{\mathrm{d}}h - \displaystyle\int_{d_{\mathrm{r}}}^{y} \tau(\xi)\mathrm{d}\xi\right] + \dfrac{e_{\mathrm{a}}}{E_{\mathrm{a}}}E_z & d_{\mathrm{r}} < y < t_{\mathrm{r}} \end{cases}. \tag{24}$$

3.3. Formulation of integral equations

The half plane to which the actuator is bonded is subjected to the following boundary conditions:

$$\tau_{yz} = \begin{cases} -\tau(y) & t_{\mathrm{l}} < y < d_{\mathrm{l}} \text{ and } d_{\mathrm{r}} < y < t_{\mathrm{r}} \\ 0 & \text{otherwise} \end{cases}. \tag{25}$$

The solution for ϵ_y can be obtained, by making use of the fundamental solution of a half space subjected to a concentrated surface force, as

$$\epsilon_y(y,0)|_{\mathrm{host}} = \frac{2}{\pi\bar{E}}\left[\int_{t_{\mathrm{l}}}^{d_{\mathrm{l}}} \frac{\tau(\xi)}{y-\xi}\,\mathrm{d}\xi + \int_{d_{\mathrm{r}}}^{t_{\mathrm{r}}} \frac{\tau(\xi)}{y-\xi}\,\mathrm{d}\xi\right]. \tag{26}$$

The compatibility of deformation between the actuator and the host structure indicates that

$$\epsilon_y|_{\mathrm{actuator}} = \epsilon_y|_{\mathrm{host}}\ t_{\mathrm{l}} < y < d_{\mathrm{l}},\ d_{\mathrm{r}} < y < t_{\mathrm{r}},\ z = 0 \tag{27}$$

and

$$u_y(d_{\mathrm{r}})|_{\mathrm{actuator}} - u_y(d_{\mathrm{l}})|_{\mathrm{actuator}} = u_y(d_{\mathrm{r}},0)|_{\mathrm{host}} - u_y(d_{\mathrm{l}},0)|_{\mathrm{host}}. \tag{28}$$

Substituting Eqs. (24) and (26) into Eq. (27) gives

$$\frac{2}{\pi\bar{E}}\int_{t_l}^{d_l}\frac{\tau(\xi)}{y-\xi}\,\mathrm{d}\xi+\frac{2}{\pi\bar{E}}\int_{d_r}^{t_r}\frac{\tau(\xi)}{y-\xi}\,\mathrm{d}\xi+\begin{cases}\dfrac{1}{hE_a}\displaystyle\int_{t_l}^{y}\tau(\xi)\mathrm{d}\xi=\dfrac{e_aE_z}{E_a} & t_l<y<d_l\\ \dfrac{1}{hE_a}\displaystyle\int_{d_r}^{y}\tau(\xi)\mathrm{d}\xi=\dfrac{e_aE_z}{E_a}+\dfrac{\sigma_d}{E_a} & d_r<y<t_r\end{cases}, \tag{29}$$

while Eq. (28) can be rewritten as

$$\frac{2}{\pi\bar{E}}\int_{d_l}^{d_r}\left\{\int_{t_l}^{d_l}\frac{\tau(\xi)}{y-\xi}\,\mathrm{d}\xi+\int_{t_l}^{d_l}\frac{\tau(\xi)}{y-\xi}\,\mathrm{d}\xi\right\}\mathrm{d}y=\frac{\sigma_d+e_aE_z}{E_a}(d_r-d_l). \tag{30}$$

Eqs. (23), (29) and (30) can be normalized as

$$\int_{-1}^{1}\frac{\tau^l(\zeta)\mathrm{d}\zeta}{\eta_l-\zeta}+\int_{-1}^{1}\frac{\tau^r(\zeta)\mathrm{d}\zeta}{\eta_r-\zeta}+\begin{cases}qv_l\displaystyle\int_{-1}^{\eta_l}\tau^l(\zeta)\mathrm{d}\zeta=1 & |\eta_l|<l\\ -qv_r\displaystyle\int_{\eta_r}^{l}\tau^r(\zeta)\mathrm{d}\zeta=1 & |\eta_r|<1\end{cases}, \tag{31}$$

$$v_l\int_{1}^{\eta*_l}\int_{-1}^{1}\frac{\tau^l(\zeta)\mathrm{d}\zeta}{\eta_l-\zeta}\,\mathrm{d}\eta_l+v_r\int_{\eta*_r}^{-1}\int_{-1}^{1}\frac{\tau^r(\zeta)\mathrm{d}\zeta}{\eta_r-\zeta}\,\mathrm{d}\eta_r=2(v-v_l-v_r)q\left[\sigma*+\frac{e_aE_z}{p}\right], \tag{32}$$

$$\int_{-1}^{1}\tau^l(\zeta)\mathrm{d}\zeta=-\frac{\sigma*}{v_l}$$

and

$$\int_{-1}^{1}\tau^r(\zeta)\mathrm{d}\zeta=\frac{\sigma*}{v_r}. \tag{33}$$

The normalized stresses are given by

$$\tau^l(\zeta)=\frac{\tau(a_l\zeta+y_l)}{p},$$

$$\tau^r(\zeta)=\frac{\tau(a_r\zeta+y_r)}{p}$$

and

$$\sigma*=\frac{\sigma_d}{p}, \tag{34}$$

with

$$\left.\begin{aligned} \eta_{\mathrm{l}} = (y - y_{\mathrm{l}})/a_{\mathrm{l}},\ \eta_{\mathrm{r}} = (y - y_{\mathrm{r}})/a_{\mathrm{r}} \\ v = a/h,\ v_{\mathrm{l}} = a_{\mathrm{l}}/h,\ v_{\mathrm{r}} = a_{\mathrm{r}}/h \\ a = \frac{1}{2}(t_{\mathrm{r}} - t_{\mathrm{l}}),\ a_{\mathrm{l}} = \frac{1}{2}(d_{\mathrm{l}} - t_{\mathrm{l}}),\ a_{\mathrm{r}} = \frac{1}{2}(t_{\mathrm{r}} - d_{\mathrm{r}}) \\ y_{\mathrm{l}} = \frac{1}{2}(d_{\mathrm{l}} + t_{\mathrm{l}}),\ y_{\mathrm{r}} = \frac{1}{2}(t_{\mathrm{r}} + d_{\mathrm{r}}) \\ \eta_{\mathrm{l}}^{*} = 2\frac{v - v_{\mathrm{r}}}{v_{\mathrm{l}}} - 1,\ \eta_{\mathrm{r}}^{*} = -2\frac{v - v_{\mathrm{l}}}{v_{\mathrm{r}}} + 1. \end{aligned}\right\} \tag{35}$$

3.4. Solution of singular integral equations

The partially debonded actuator can be regarded as two 'actuators' subjected to an axial stress σ_{d} at their inner tips, as shown in Fig. 4. Since the application of σ_{d} will not change the singular behaviour of the solution, the interfacial shear stress at the tips of these 'actuators' will also be square-root singular. Therefore, the general solutions of τ^{l} and τ^{r}, in Eqs. (31)–(33), can then be expressed in terms of the following expansions of the Chebyshev polynomials,

$$\tau^{\mathrm{l}}(\eta_{\mathrm{l}}) = \frac{1}{\sqrt{1-\eta_{\mathrm{l}}^2}} \sum_{j=0}^{\infty} d_j^{\mathrm{l}} T_j(\eta_{\mathrm{l}})$$

and

$$\tau^{r}(\eta_{\mathrm{r}}) = \frac{1}{\sqrt{1-\eta_{\mathrm{r}}^2}} \sum_{j=0}^{\infty} d_j^{r} T_j(\eta_{\mathrm{r}}). \tag{36}$$

If the Chebyshev polynomial expansions are truncated to the Nth term, and Eq. (31) is satisfied at the following collocation points at each bonded segment of the actuator given by

$$\eta_{\mathrm{l}k} = \eta_{\mathrm{r}k} = \eta_k = \cos\frac{k-1}{N-1}\pi,\ k = 1,2,\ldots,N, \tag{37}$$

Eq. (31) reduces to

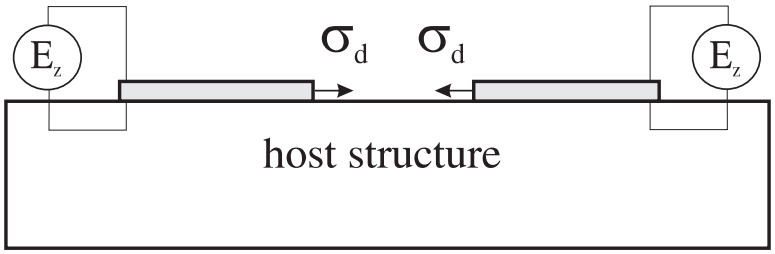

Fig. 4. Equivalent model of a partially debonded actuator.

$$\sum_{j=1}^{N} d_j^1 \frac{\sin\left(j\frac{k-1}{N-1}\pi\right)}{\sin\left(\frac{k-1}{N-1}\pi\right)}\left[1+\frac{qv_1}{\pi j}\sin\left(\frac{k-1}{N-1}\pi\right)\right]+\sum_{j=1}^{N} d_j^r\left[\left(\eta_k^2-1\right)^{1/2}+\eta_k\right]^j \Big/ \sqrt{\eta_k^2-1}$$
$$+\frac{\sigma*}{\pi}\left\{\frac{1}{v_r\sqrt{\eta_k^2-1}}+q\left[1-\frac{k-1}{N-1}\right]\right\}=-\frac{1}{\pi}, \tag{38}$$
$$k=1,2,\ldots,N$$

and

$$\sum_{j=1}^{N} d_j^r \frac{\sin\left(j\frac{k-1}{N-1}\pi\right)}{\sin\left(\frac{k-1}{N-1}\pi\right)}\left[1+\frac{qv_r}{\pi j}\sin\left(\frac{k-1}{N-1}\pi\right)\right]-\sum_{j=1}^{N} d_j^1(-1)^j\left[\left(\eta_k^2-1\right)^{1/2}+\eta_k\right]^j \Big/ \sqrt{\eta_k^2-1}$$
$$+\frac{\sigma^*}{\pi}\left\{\frac{1}{v_1\sqrt{\eta_k^2-1}}+q\frac{k-1}{N-1}\right\}=-\frac{1}{\pi}, \tag{39}$$
$$k=1,2,\ldots,N$$

In addition, Eq. (32) becomes

$$\sigma^*\left\{-\ln\left[\left|\eta_1^*+\sqrt{\eta_1^{*2}-1}\right|\left|\eta_r^*+\sqrt{\eta_r^{*2}-1}\right|\right]-2(v-v_1-v_r)q\right\}+\sum_{j=1}^{N} d_j^1\left\{\pi v_1(-1)^j\int_1^{\eta_1^*}\right.$$
$$\left.\times\left[\left(\eta_1^2-1\right)^{1/2}-\eta_1\right]^j\Big/\sqrt{\eta_1^2-1}\,\mathrm{d}\eta_1\right\}+\sum_{j=1}^{N} d_j^r\left\{-\pi v_r\int_{\eta_r^*}^{-1}\left[\left(\eta_r^2-1\right)^{1/2}-\eta_r\right]^j\Big/\sqrt{\eta_r^2-1}\,\mathrm{d}\eta_r\right\} \tag{40}$$
$$=2(v-v_1-v_r).$$

From these equations, the unknown coefficients d_j^1 and d_j^r can be determined. The resulting SSSF at the left and the right tips of the actuator can be expressed in terms of d_j^1 and d_j^r as

$$S_1=p\sqrt{a_1\pi}\sum_{j=0}^{N}(-1)^j d_j^1$$

and

$$S_r=p\sqrt{a_r\pi}\sum_{j=0}^{N} d_j^r. \tag{41}$$

In addition, the SSSFs at the left and the right ends of the debonding part can be obtained as

$$S_{\mathrm{dl}} = p\sqrt{a_{\mathrm{l}}\pi}\sum_{j=0}^{N} d_j^{\mathrm{l}}$$

and

$$S_{\mathrm{dr}} = p\sqrt{a_r\pi}\sum_{j=0}^{N}(-1)^j d_j^{\mathrm{r}}. \tag{42}$$

4. The singular behaviour of an interfacial crack

It should be noted that the existence of a square root singularity at the tips of the actuator is based upon the electromechanical line model. However, the resulting SSSF can be related to the singular behaviour of the interfacial crack due to interfacial debonding. Such a relation can be established by using path independent integral in the current composite piezoelectric media.

4.1. Conservative path integral in piezoelectric composites

Pak (1990) introduced a path integral in piezoelectric materials by taking the electric enthalpy density to be the Lagrangian density of the considered system. The path integral is defined by

$$J = \int_{\Gamma}\left\{H\,\mathrm{d}z - \left(T_j\frac{\partial u_j}{\partial y} + D\frac{\partial \phi}{\partial y}\right)\mathrm{d}s\right\}, \tag{43}$$

with

$$T_i = \sigma_{ij}n_j,\ D = D_i n_i, \tag{44}$$

where ϕ is the electric potentialand Γ is the integration path, with n_j being the outward normal of Γ and

$$H = \frac{1}{2}\sigma_{ij}\epsilon_{ij} - \frac{1}{2}D_i E_i \tag{45}$$

being the electric enthalpy density. σ_{ij}, ϵ_{ij}, D_i and E_i are the stresses, strains, electric displacements and electric field intensities. This integral vanishes when it surrounds a perfect piezoelectric material, which is free of defects and inhomogeneities without body forces and free charges.

The integral defined in Eq. (43) can be further extended into cases involving dissimilar piezoelectric media bonded together through straight interfaces. For two bonded piezoelectric materials (Fig. 5), consider two separate closed loops given by

$$\Gamma_+ = \Gamma_1 + \Gamma_{\mathrm{I}+}$$

and

$$\Gamma_- = \Gamma_2 + \Gamma_{\mathrm{I}-}, \tag{46}$$

with $\Gamma_{\mathrm{I}+}$ and $\Gamma_{\mathrm{I}-}$ sharing the same region of the interface and being in the upper and the lower parts, respectively. The conservative behaviour of the path integral for closed loops implies the existence of the following relations,

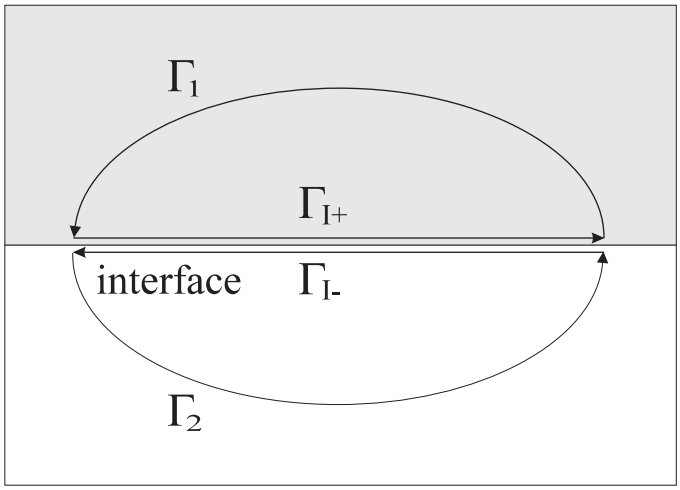

Fig. 5. Integral path including a material interface.

$$J_{\Gamma_+} + J_{\Gamma_-} = J_{\Gamma_1} + J_{\Gamma_2} + J_{\Gamma_{I+}} + J_{\Gamma_{I-}} = 0. \tag{47}$$

Since the two bonded piezoelectric media should satisfy the continuity conditions along the interface, i.e.,

$$T_i^+ = -T_i^-,$$

$$D^+ = -D^-,$$

$$u_i^+ = u_i^-$$

and

$$\phi^+ = \phi^-, \tag{48}$$

the following relation can be obtained,

$$J_{\Gamma_0} = J_{\Gamma_1} + J_{\Gamma_2} = 0. \tag{49}$$

This result indicates that for any closed loop $\Gamma_0 = \Gamma_1 + \Gamma_2$, which includes part of the interface, $J_{\Gamma_0} = 0$.

4.2. Path integral around an interfacial crack

Let us consider now the case of a piezoelectric actuator which is debonded at the edge to a host elastic solid, as shown in Fig. 6. According to the conservative property of J, the integral along the closed loop shown in Fig. 6 will be zero, i.e.,

$$J_{\Gamma_{\text{out}}} + J_{\Gamma_{\text{top}}} + J_{\Gamma_{\text{end}}} + J_{\Gamma_{c+}} + J_{\Gamma_{\text{tip}}} + J_{\Gamma_{c-}} = 0, \tag{50}$$

with Γ_{out} being the path from A to C, Γ_{top} and Γ_{end} along the top and the end of the actuator, Γ_{c+} and Γ_{c-} being along the upper and lower surfaces of the crack, and Γ_{tip} around the tip of the crack.

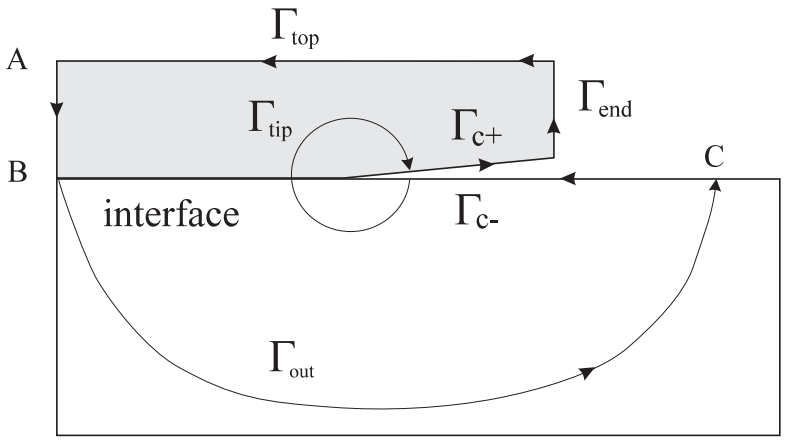

Fig. 6. Integral path around an interfacial debonding.

By making use of the boundary conditions that the traction and the electrical displacement at the top surface and the crack surfaces are zero, the above relations can be reduced to

$$J_{\Gamma_{\text{out}}} + J_{\Gamma_{\text{end}}} + J_{\Gamma_{\text{tip}}} = 0. \tag{51}$$

If the crack is much longer than the thickness of the actuator, the end of the actuator can be assumed to be mechanically free, i.e., σ_{ij} can be assumed to be zero. According to this condition, $J_{\Gamma_{\text{end}}}$ can be obtained as

$$J_{\Gamma_{\text{end}}} = -\frac{1}{2}\left(\epsilon_{\text{a}} + \frac{e_{\text{a}}^2}{E_{\text{a}}}\right)E_z^2. \tag{52}$$

4.3. Path integral around an actuator

For the case where the actuator is very thin, the stress field far from the end of a debonded actuator can be predicted by the current actuator model.

Therefore, the path integral $J_{\Gamma_{\text{out}}}$ in Eq. (52) can be determined by using the stress field predicted by the actuator model. As shown in Fig. 7, $J_{\Gamma_{\text{out}}}$ can be divided into two parts, i.e.,

$$J_{\Gamma_{\text{out}}} = J_{\bar{\Gamma}_{\text{out}}} + J_{\Gamma_{AB}}, \tag{53}$$

where $\bar{\Gamma}_{\text{out}}$ is a path from B to C, which is far from the end of the debonding, Γ_{AB} is a path across the thickness of the actuator from A to B. By using the actuator model, $J_{\Gamma_{AB}}$ can be reduced to

$$J_{\Gamma_{AB}} = \frac{1}{2}hE_{\text{a}}\epsilon_y^2|_B + \frac{1}{2}h\epsilon_{\text{a}}E_z^2, \tag{54}$$

where ϵ_{a} is the dielectric constant of the actuator given in Appendix A.

$J_{\bar{\Gamma}_{\text{out}}}$ can further be related to the singular field at the tip of the actuator. Let us consider a closed loop in the host material, as shown in Fig. 8. The conservative behaviour of the path integral indicates that

$$J_{\bar{\Gamma}_{\text{out}}} + J_{\bar{\Gamma}_{\text{tip}}} + J_{\Gamma_{\text{a}-}} = 0, \tag{55}$$

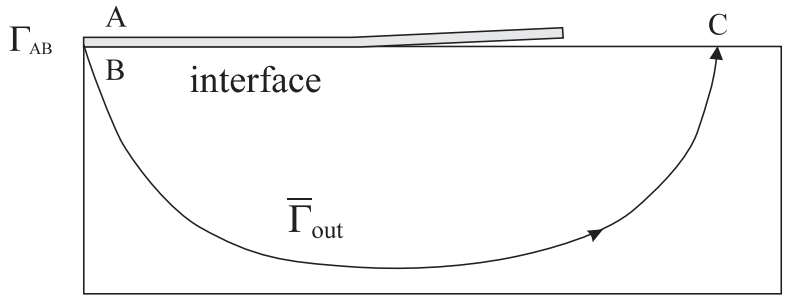

Fig. 7. Path integral using the actuator model.

in which

$$J_{\Gamma_{a-}} = \int_D^B \tau \epsilon_y \, dy, \tag{56}$$

with τ being the interfacial shear stress between the actuator and the host, shown in Fig. 2. By using Eqs. (1) and (5), the above integral can be obtained as

$$J_{\Gamma_{a-}} = -\frac{1}{2} h E_a \left(\epsilon_y^2|_D - \epsilon_y^2|_B \right). \tag{57}$$

Therefore, Eq. (55) reduces to

$$J_{\bar{\Gamma}_{out}} = -J_{\bar{\Gamma}_{tip}} + \frac{1}{2} h E_a \left(\epsilon_y^2|_D - \epsilon_y^2|_B \right). \tag{58}$$

Substituting Eqs. (58) and (54) into Eq. (53) gives

$$J_{\Gamma_{out}} = -J_{\bar{\Gamma}_{tip}} + \frac{1}{2} h E_a \epsilon_y^2|_D + \frac{1}{2} h \epsilon_a E_z^2. \tag{59}$$

According to the actuator model, the axial stress of the actuator is zero at the tip of the debonding region, as given by Eq. (2). When point D approaches this tip, the corresponding axial strain $\epsilon_y|_D$ can be determined using the constitutive relation of the actuator Eq. (5) as

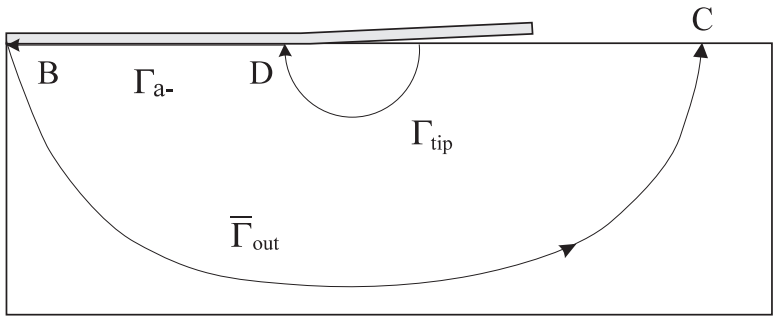

Fig. 8. Integral path in the host material.

$$\epsilon_y|_D = \frac{e_a}{E_a} E_z. \tag{60}$$

Therefore, by substituting Eqs. (59), (60) and (52) into Eq. (51), the path integral around the tip of the original interfacial crack can be obtained as

$$J_{\Gamma_{tip}} = J_{\bar{\Gamma}_{tip}}. \tag{61}$$

By making use of the asymptotic stress and displacement fields near the tip of the debonding region, the above integral can be further expressed in terms of the shear stress singularity factor, such that

$$J_{\Gamma_{tip}} = -\frac{S^2}{128E\pi}\left[(22+3\nu)\pi + \frac{760}{7}(1+\nu)\right]. \tag{62}$$

This result represents the relation between the path integral around the tip of the real interfacial crack and SSSF associated with the actuator model. It can then be concluded that the SSSF obtained from the present actuator model is indeed representative of the singular behaviour of the interfacial debonding process.

5. Numerical examples and discussions

5.1. Shear stress singularity factor of a perfectly bonded actuator

Fig. 9 shows the normalized shear stress singularity factor, $S^* = -S/p'\sqrt{2\pi h}$, of a perfectly bonded actuator. The behaviour of this composite structure is governed by three parameters, q', v and p', given by Eqs. (15) and (16). It is interesting to observe that with the increase of $v = a/h$, S^* increases and approaches a constant which corresponds to the case of an infinitely long actuator.

5.2. Stress distribution at the interface

The interfacial shear stress, which transfers the actuation energy between the actuator and the host structure, can be determined directly from the solution given in the previous section. Fig. 10 shows a typical shear stress distribution of a surface bonded actuator for $q = 2.28$ and $v = 5.0$, where $\tau^* = \tau_{yz}(y,0)/p$.

To verify the validity of the present actuator model to predict the interfacial stress distribution, the ANSYS software was used to numerically analyze the stress field of the same problem using the real geometric configuration of the actuator. The comparison shows a limited discrepancy between the finite element and analytical results near the tips of the actuator. This discrepancy is caused by the use of different actuator models in the analyses. In the analytical work, one-dimensional representation was used to model the behaviour of the actuator, while in the finite element analysis a two-dimensional model was used. The current one-dimensional actuator model can be used to predict interfacial shear stress 'far' from the tips of the actuator (two times of the thickness of the actuator, for example). However, it should be mentioned that most sheet-actuators have high length-to-thickness ratio. In these situations, the current explicit model can be used to predict the load transfer between the actuator and the host structure analytically in an efficient manner.

5.3. SSSF due to edge debonding

The high shear stress concentration at the edges of the actuator may result in an interfacial debonding

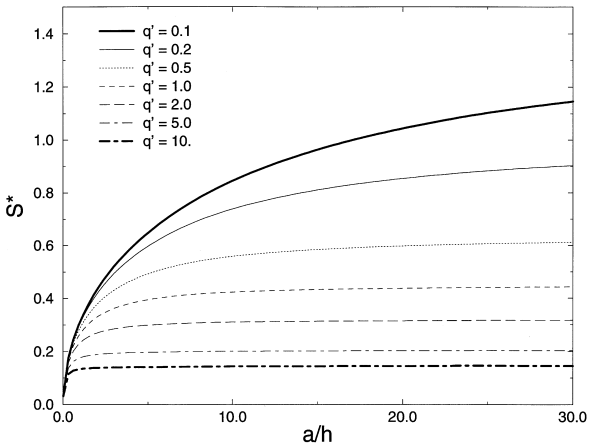

Fig. 9. Normalized SSSF of a single actuator.

of length d, as shown in Fig. 11. As mentioned in Section 3.1, a debonded actuator can be regarded as a shorter actuator. Therefore, the effective length of the actuator is reduced from its original length $2a$ to $2a_{\text{eff}}=2a-d$. It is interesting to note that with the growth of debonded length, the shear stress singularity factor S decreases. When S reaches the 'interfacial toughness' S_c, the debonding will stop growing, as illustrated in Fig. 12. This result indicates that an edge debonding will self-arrest following a period of growth leading to a reduction in the effective length of the actuator to a_c.

5.4. SSSF due to central debonding

The imperfect bonding in the fabrication process of smart structures may also result in interfacial debonding between the actuator and the host structure. For the general case of central debonding (Fig. 13), the debonded part will not experience interfacial shear stresses. However, its actuation effect upon the structure will not disappear, as in the case of edge debonding. In this case, the debonded region will

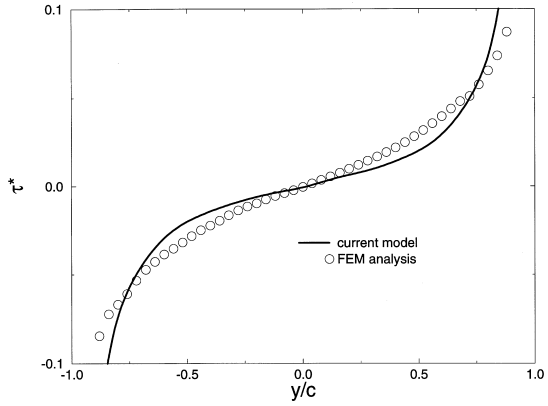

Fig. 10. Interfacial shear stress distribution.

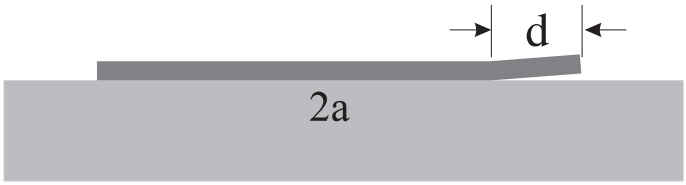

Fig. 11. Edge debonding of an actuator.

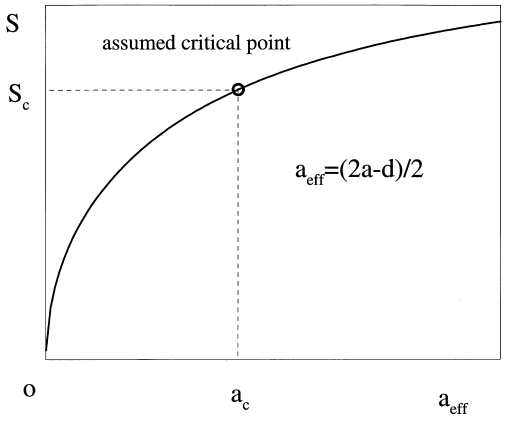

Fig. 12. Self-arrest of edge debonding.

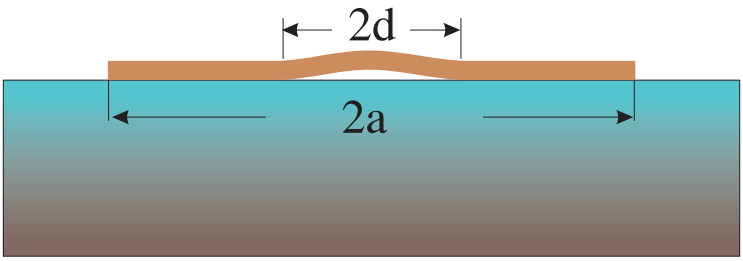

Fig. 13. Central debonding of an actuator.

affect the structure by applying an axial stress to the remaining parts of the actuator. Fig. 14 shows the normalized quasistatic shear stress singularity factor $S^* = -S/p\sqrt{\pi h}$ due to a symmetric central debonding. A significant increase of S^* is observed when the tip of the debonded region approaches the end of the actuator. Fig. 15 shows the normalized axial stress $\sigma^* = -\sigma_d/p$, in the debonded part of the actuator.

6. Concluding remarks

A general analytical solution is provided to the coupled electromechanical behaviour of a piezoelectric

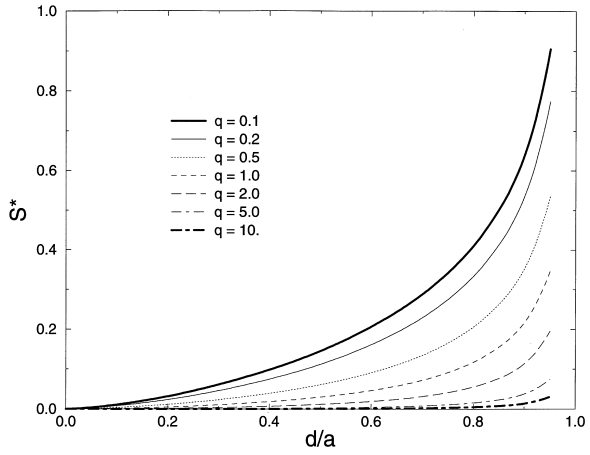

Fig. 14. The SSSF of a centrally-debonded actuator.

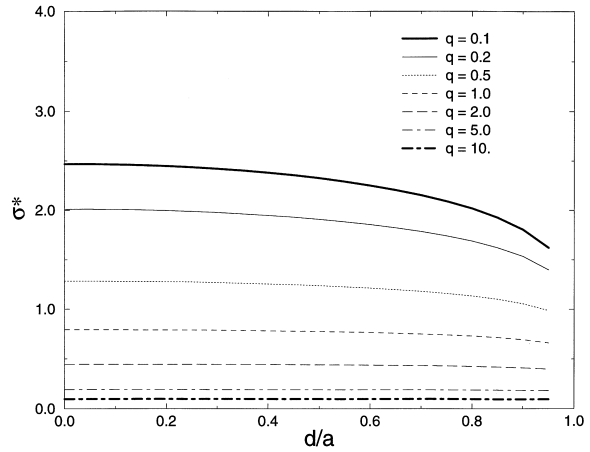

Fig. 15. The normal stress in a centrally-debonded actuator.

actuator bonded to a host under plane electric loading. The analysis is based upon the use of a piezoelectric line model of the actuator which reduces the problem to the solution of singular integral equations of the first kind. The newly defined shear stress singularity factor provides a description of the local stress field around the tip of the actuator, which represents the singular behaviour of the interfacial crack.

The validity of the present model hase been demonstrated by application to specific examples and comparison with the correspond results obtained from Finite Element method. Furthermore, the effect of the shape of the actuator, the material combination and the electromechanical coupling upon the resulting shear stress singularity factor of the actuator are examined and discussed.

Acknowledgements

This work was supported in part by the Natural Sciences and Engineering research Council of Canada. The authors wish to thank one of the reviewers for his/her constructive remarks.

Appendix A. Effective material constants

The mechanical and electrical properties of piezoceramic materials can be described fully by:
The equation of motion

$$\sigma_{ji,j} + f_i = \rho \ddot{u}_i.$$

Gauss' law

$$D_{i,i} = 0.$$

The constitutive equations

$$\{\sigma\} = [c]\{\epsilon\} - [e]\{E\}, \{D\} = [e]\{\epsilon\} + [\epsilon]\{E\},$$

where

$$\epsilon_{ij} = \frac{1}{2}(u_{i,j} + u_{j,i}), E_i = -V_{,i}.$$

In these equations, $\{\sigma\}$ and $\{\epsilon\}$ are the stress and the strain fields, f_i and ρ are the body force and the mass density, while $\{D\}$, $\{E\}$ and V represent the electric displacement, the electric field intensity and the potential, respectively. $[c]$ is a matrix containing the elastic stiffness parameters for a constant electric potential, $[e]$ represents a tensor containing the piezoelectric constants and $[\epsilon]$ represents the dielectric constants for zero strains.

According to the electroelastic line actuator model, the effective material constants of the actuator model are given by

$$E_a = c_{11} - \frac{c_{13}^2}{c_{33}} \text{ plane strain,}$$

$$e_a = e_{13} - e_{33}\frac{c_{13}}{c_{33}} \text{ plane strain}$$

and

$$\epsilon_a = \epsilon_{33} + \frac{e_{33}^2}{c_{33}} \text{ plane strain,}$$

where the direction of polarization is designated as being the z-axis.

References

Benveniste, Y., 1992. The determination of the elastic and electric fields in a piezoelectric inhomogeneity. J. Appl. Phys. 72, 1086–1095.

Cox, H.L., 1952. The elasticity and strength of paper and other fibrous materials. Brit. J. Appl. Phys. 3, 72–79.
Crawley, E.F., Anderson, E.H., 1990. Detailed models of piezoelectric actuation of beams. Journal of Intelligent Material systems and Strctures 1, 4–25.
Crawley, E.F., de Luis, J., 1987. Use of piezoelectric actuators as elements of intelligent structures. AIAA Journal 25, 1373–1385.
Deeg, W.F., 1980. The analysis of dislocation, crack and inclusion problems in piezoelectric solids, Ph.D. dissertation, Stanford University.
Dosch, J., Lesieutre, G., Koopmann, G., Davis, C., 1995. Inertial piezoceramic actuators for smart structures. SPIE 2447, 14–25.
Dunn, M., Taya, M., 1993. Micromechanical predictions of the effective electro–elastic moduli of piezoelectric composites. Int. J. Solid Struct. 30, 161–175.
Fukuda, H., Chou, T.W., 1981. An advanced shear lag model applicable to discontinuous fiber composites. J. Comp. Mat. 15, 79–91.
Gandhi, M.V., Thompson, B.S., 1992. Smart Materials and Structures. Chapman & Hall, London.
He, M.-Y., Suo, Z., McMeeking, R.M., Evans, A.G., Lynch, C.S., 1994. The mechanics of some degradation mechanisms in ferroelectric ceramic actuators. SPIE 2189, 344–356.
Hubbard, J.E., Bailey, T., 1985. Distributed piezoelectric–polymer active vibration control of a cantilever beam. Journal of Guidance, Control, and Dynamics 8, 605–611.
Im, S., Atluri, S.N., 1989. Effects of a piezo-actuator on a finite deformation beam subjected to general loading. AIAA Journal 27, 1801–1807.
Jain, A.K., Sirkis, J.S., 1994. Continuum damage mechanics in piezoelectric ceramics, Adaptive Structures and Composite Materials: Analysis and Application. ASME 45/54, 47–58.
Lin, M.W., Rogers, C.A., 1993a. Modeling of the actuation mechanism in a beam structure with induced strain actuators. In: Proceedings of AIAA/ASCE/ASME/ASC 34th Structures, Structural Dynamics and Materials Conference, Part VI. AIAA Inc, Washington, DC, pp. 3608–3617 La Jolla, CA. 19–22 April 1993.
Lin, M.W., Rogers, C.A., 1993b. Actuation response of a beam structure with induced strain actuators. Adaptive Structures and Material Systems 35, 129–139.
Muskhelishvili, N.I., 1953. Some Basic Problems of the Mathematical Theory of Elasticity. Noordhoff, Groningen.
Pak, Y.E., 1990. Crack extension force in a piezoelectric material. J. Appl. Mech. 57, 647–653.
Varadan, V.K., Wu, Z., Bao, X.-Q., Varadan, V.V., 1993. Light weight robot using piezoelectric motor, sensor and actuator. Adaptive Structures and Material Systems 35, 141–148.